Simplifying calibration of bonded elasto-plastic models

Sara Rios, PhD
Post-Doc research fellow, CONSTRUCT-GEO, Faculty of Engineering (FEUP), University of Porto, Portugal (sara.rios@fe.up.pt)

Matteo Ciantia, PhD
Post-Doc research fellow, Departamento de Ingeniería del Terreno, Universidad Politécnica de Cataluña, Barcelona, Spain (matteo.ciantia@upc.edu)

Nubia Gonzalez, PhD
Research Engineer, REPSOL I+D, Madrid, Spain nubiaaurora.gonzalez@repsol.com

Marcos Arroyo, PhD
Associate Professor, Departamento de Ingeniería del Terreno, Universidad Politécnica de Cataluña, Barcelona, Spain (marcos.arroyo@upc.edu)

António Viana da Fonseca
Associate Professor, CONSTRUCT-GEO, Faculty of Engineering (FEUP), University of Porto, Portugal (viana@fe.up.pt)

Keywords: Constitutive model; cemented sand; porosity-cement ratio; CASM model; high pressure triaxial tests

Abstract

Using realistic constitutive models for artificially cemented soils is advantageous in design. However, the price of that increased realism is often a more elaborate model, which is difficult to calibrate. A database of high quality triaxial tests on compacted cemented silty sand is used to calibrate and validate a generalized critical state bonded soil model. The exercise highlights the staged calibration procedure that is convenient in this kind of application. The calibration results have shown a direct relation between added yield strength and a well-established soil-cement mixture ratio, which facilitates the application of the model in design. It is shown that such relation can be also deduced from the analysis of unconfined compressive strength tests.

Introduction

Artificially cemented soils are extensively used in a variety of geotechnical engineering applications. Cement improved soils are generally stronger and stiffer but more brittle than the parent soil. The effects of stress level and strain history on stiffness and strength are modified by the presence of cement. Broadly speaking, strain-hardening soils are transformed into strain-softening materials. Densification, which is generally positive for non-cemented soils, might become undesirable after treatment.

Accurate modelling of the mechanical behaviour of improved soil is important, either because they directly have some structural role (e.g. soil-cement columns beneath an embankment) or because mechanical integrity is a prerequisite for its function (e.g. an isolating barrier for a contaminated zone). Many practical rules and approximate solutions are available for design of structures incorporating improved soils (e.g. [1]). However, when some circumstance makes those rules inapplicable or uneconomical, numerical analysis will be typically required.

How to represent the mechanical behaviour of the improved soil in numerical analysis is subject to some debate. Treated soils are intermediate materials between soils and rocks and several analogies are possible. For instance, elasto-plastic Mohr-Coulomb models incorporating residual strength such as those used for rocks (e.g. [2]) have been applied to model cement treated clay ([3]). Similarly, and because improved soils have analogies with concrete, cemented soils have been represented adapting models originally developed for concrete [4]. Taking a different perspective, a number of researchers have successfully extended elasto-plastic models for soils of the critical state tradition to represent artificially cemented clays [5] and silts [6]. This approach is directly inspired by a long line of constitutive models originally developed for naturally structured soils and soft rocks ([7], [8] , [9], [10])

Despite all those developments it is fair to say that simplified, elastic perfectly plastic models (with either a Mohr-Coulomb or Tresca failure criterion) still dominate numerical applications (e.g. [11], [12]). It is accepted that this type of model may neglect many important features of cemented soil behaviour, but it appears easy to calibrate. Alternative material models, which may represent with more accuracy the target behaviour, are perceived as difficult to calibrate, particularly when the practical constraints of treated soil investigation are noted (limited "in situ" testing; dominance of simple tests like UCS -Unconfined Compressive Strength).

Indeed, if calibration procedures remain difficult, there will be very limited use of advanced constitutive models in practice. That may be disadvantageous, because several examples ([5], [3]) show that structure-scale responses predicted numerically are strongly dependent on the constitutive model and that elastic-perfectly plastic models may not capture all relevant failure modes.

To address this problem, models that are not just accurate but also as simple to calibrate as possible are necessary. The purpose of this work is to contribute to that goal of simplified calibration. A bonded elasto-plastic constitutive model, previously used to simulate cemented Bangkok clay [5] behaviour, is here used for a very different cemented soil, namely compacted cemented silty sand. While the Bangkok clay case was representative of products obtained by

deep mixing "in situ", the case presented here is representative of the cemented soils used within engineered fills. In what follows, after introducing the constitutive model and the target material, the calibration process is described, extracting general lessons that will facilitate further application of bonded elasto-plastic models.

Case description

Constitutive model

The constitutive model formulation is based on the original model for clays and sands (CASM) developed by [13]. CASM is an elasto-plastic single surface model of the critical state tradition that has been used as a starting point to develop more advanced soil models by several researchers ([6], [14] and [15]). The model applied in this work, called herein "Cemented CASM" (C-CASM) is part of a suite of advanced models based on CASM that are described in [16]. This model has already been successfully applied to clays, both naturally structured ([17] and [18]), and artificially cemented [5]. However, it is the first time a cemented granular soil is calibrated with this model.

C-CASM extends CASM introducing a new basic state variable, b, to represent the intact amount of intergranular bonding as defined by [19]. The shape of the yield surface is assumed to be the same in uncemented and cemented conditions. Bonding (b) modifies the yield surface, enlarging it with increasing amount of cementation. The way the yield surface is affected by bonding (b) is expressed using two separate intermediate or derived state variables, p'_c and p'_t, which control respectively the isotropic compression yield and the tensile yield of the soil (Figure 1). These intermediate variables are:

$$p'_c = p'_s \left(1 + b \right) \tag{1}$$

$$p'_t = \alpha \, p'_s b \tag{2}$$

where p'_s is the equivalent preconsolidation pressure, and α is a model parameter, controlling the tensile strength derived from cementation (see Figure 1).
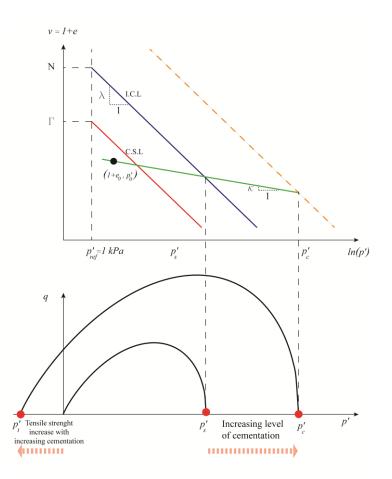
Figure 1 Compression plane including reference lines (Isotropic Compression Line, ICL; Critical State Line, CSL) and yield surface on the triaxial plane.

The yield surface is given by equation (3),

$$f = \left(\frac{q}{M \left(p' + p'_t \right)} \right)^{\bar{n}} + \frac{1}{\ln r} \left(\frac{p' + p'_t}{p'_c + p'_t} \right) \tag{3}$$

where M is the stress-ratio (q/p') at critical state. Several flow rules can be implemented in C-CASM. Rowe stress-dilatancy relationship is used here,

$$d = \frac{\dot{\varepsilon}_v^p}{\dot{\varepsilon}_q^p} = \frac{9 \left(M - \eta \right)}{9 + 3M - 2M \eta} \tag{4}$$

Where $\dot{\varepsilon}_v^p$ is the incremental plastic volumetric strain and $\dot{\varepsilon}_q^p$ the incremental plastic shear strain.

The equivalent preconsolidation pressure evolves following the classical critical state hardening rule,

$$\frac{\dot{p}'_s}{p'_s} = \frac{\dot{v}}{\lambda - \kappa} \tag{5}$$

λ and κ are compressibility parameters of the reference material (Figure 1).

 Following [19] bonding b is degraded exponentially with accumulated plastic damage h,

$$b = b_0 e^{-h} \tag{6}$$

$$\dot{h} = h_1 \dot{\varepsilon}_v^p + h_2 \dot{\varepsilon}_q^p \tag{7}$$

where b_0 is the initial bonding and h_1 and h_2 are two material parameters. The elastic stiffness for cemented materials is made dependent on bonding [15],

$$\kappa_c = \frac{\kappa}{1 + \sqrt{\frac{p'_s b}{p}}} \tag{8}$$

The model requires specification of 10 parameters, seven of which describe the reference uncemented material, and initialization of two state variables, apart from effective stress.

A version of C-CASM valid for general stress paths and requiring no further parameters was coded into the finite element code PLAXIS, which has a facility to implement user-defined (UD) soil models. Further details can be found in [16].

Compacted cemented silty sand

Several cemented granular materials were created by mixing cement, water and a silty sand, weathering product of Porto granite. This is a well characterized soil and extensive geotechnical data has been gathered both for the parent soil alone [20] and for its mixtures with cement ([21], [22], [23] and [24]).

The calibration presented here uses a series of 38 triaxial tests on soil-cement mixtures The series includes isotropic, undrained and drained triaxial compression tests performed on soil-cement mixtures obtained using percentages of Portland cement (CEM I 52.5 R) between 0% and 7% of the soil dry weight. Two separate ranges of isotropic confining pressures were applied: in the low pressures 30, 80, 100 and 250 kPa were used while for the high pressures the specimens were submitted to 10 and 20 MPa. Specimens for testing were obtained by static compaction immediately after mixing covering a range of initial void ratios between 0.58 and 0.78. Initial void ratio and cement content were selected so that mixture ratio parameter ($n/C_{iv}^{0.21}$) values were clustered in two groups, around 30 and 40. The test conditions of every test are tabulated within the supplementary material to this paper; more detail on the experimental procedures and results can be found in [21]. Here it is just recalled that two different laboratories were involved, (one for low pressure tests, another for high pressure tests), and that all cemented samples showed clear signs of shear localization after dismounting.

Calibration process

Introduction

Because of the relatively large database that is available here different strategies for calibration may be adopted. A staged approach is applied, as follows:

1. Definition of a procedure for initialization of the CASM state variable, p'_s
2. Calibration of the basic CASM parameters for the uncemented, reference material (ν, κ, N, λ and M)
3. Calibration of the advanced CASM parameters for the uncemented, reference material. These are the two parameters controlling the shape of yield surface (r and $\bar{n}$)
4. Definition of a procedure for initialization of the "bond" state variable, *b*, introduced in C-CASM for cemented materials
5. Calibration of the parameters that are exclusive of cemented materials in C-CASM (h_1, h_2 and α)

The idea behind this sequential procedure is to keep separate different tasks that may require each a different amount and type of data. This may enable potential users of the model, perhaps dealing with a more limited database, to easily judge which stages of the present procedure they may follow and which they may eventually skip, by adopting some default assumption.

CASM: Initialization of p_s

For a given specimen or soil element p'_{s0} is the initial value of the equivalent preconsolidation pressure obtained from the intersection of ICL of the uncemented soil and the swelling line that passes by the point defining initial state (e_0; p'_0). Formally this is given by equation (9),

$$p'_{s0} = \exp\left(\frac{N - (1 + e_0) - \kappa \ln p'_0}{\lambda - \kappa} \right) \tag{9}$$

For compacted soils the initial void ratio value, e_0, is well known. For cemented soils that are not cured under stress, such as those in this database, there is more difficulty on judging which is the relevant effective pressure at origin, p'_0 . During specimen formation the soil is unsaturated, but suction is then relaxed by saturation before triaxial testing. As curing occurs in an 'unloaded' state, the approach followed here is to use as p'_0 the same reference pressure value that gives N on the ICL (i.e. $p'_0 = p'_{ref} = 1$ kPa).

Basic CASM parameters

Basic CASM parameters are those shared with classical critical state models such as Cam-clay. These include, M, the stress ratio (q/p') at critical state; λ, slope of the ICL (or NCL, or CSL) on the compression plane; κ, slope of the swelling line; N, the specific volume on the ICL at the reference pressure ($p_{ref} = 1$ kPa) and ν, the Poisson ratio. Values of λ, k and N were obtained fitting an isotropic compression test on uncemented material [21].

Critical state friction M was obtained as the value of zero dilatancy on a stress-dilatancy plot (Figure 2) of triaxial results on uncemented specimens. The same plot suggested that the Rowe dilatancy formulation shows a good adjustment to the results. Poisson ratio was estimated as 0.3. All the values selected for these basic parameters are summarized in Table 1.
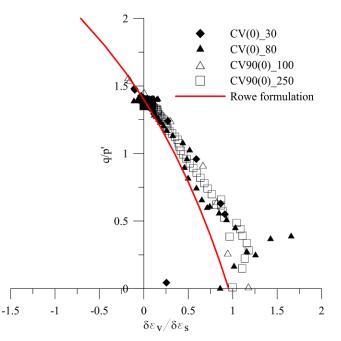

Figure 2 Stress-dilatancy results from drained triaxial tests performed on the uncemented specimens and Rowe formulation

Table 1 CASM basic (critical state) parameter set for Porto silty sand

κ	λ	N	M	υ
0.0097	0.112	2.35	1.4	0.3

Advanced CASM parameters: yield locus shape

Here are called advanced CASM parameters those that are not shared with Cam-clay models i.e. parameters (r and $\bar{n}$) controlling the yield surface shape. Yield points were identified by joint inspection of volumetric and axial deformation response in drained tests or, with more difficulty, of pore pressure and axial deformation in undrained tests (see examples in Figure 4 and Figure 5). Yield stresses were normalized by the equivalent preconsolidation pressure of each specimen. In this normalized space (Figure 3) a qualitative indication of yield surface shape is also given by undrained stress paths after yielding.

Table 2 presents the equivalent preconsolidation pressure p'_{s0} estimated for the uncemented compacted specimens using equation (9). The initial void ratios were slightly variable across specimens; to simplify two representative values (0.75 and 0.60) have been selected. Results from an uncompacted specimen, isotropically compressed to 10 MPa and then sheared undrained were also available. As indicated in Table 2 this specimen is assumed normally consolidated.

Table 2 Model state variables and initial values for triaxial tests – uncemented specimens

Name	Type	e_0	p'_{s0} (kPa)	p' (kPa)	p' / p'_{s0}
CV(0)_30	drained	0.75	359.5	30	0.08
CIU(0)_30	drained	0.75	359.5	30	0.08
CV(0)_80	drained	0.75	359.5	80	0.22
CIU(0)_250	undrained	0.75	359.5	250	0.70
CV90(0)_30	drained	0.6	1558	30	0.02
CIU90(0)_30	drained	0.6	1558	30	0.02
CV90(0)_100	drained	0.6	1558	100	0.06
HCIU(0)_1000	undrained	1.21*	10000	10000	1

*Uncompacted specimen. Void ratio value before isotropic compression

Figure 3 illustrates that most of the data available here clustered on the "dry" side. Such data leaves relatively unconstrained the shape parameter $\overline{n}$, with several values giving an adequate fit, as illustrated. It was only after inspecting the scarce results from undrained tests at high pressures that a value ($\overline{n}$ = 2.2) was finally selected. Published calibrations on CASM-based models for other soils ([5], [6], [13] and [17]) suggest a range for $\overline{n}$ between 1 and 3 and for r between 1 and 3.
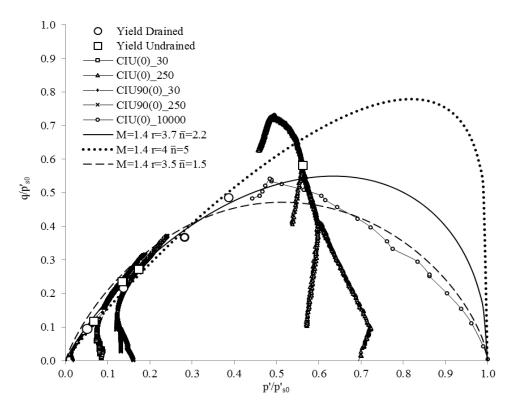

Figure 3 Normalized plot for the yield stress points of drained and undrained tests of uncemented specimens

Performance of CASM for uncemented specimens

At this stage, as summarized in Table 3, all the CASM model parameters had been selected. An example of its performance for drained and undrained tests is presented in Figure 4 and Figure 5, respectively. In general, the model adjusted reasonably to the test results. Perhaps the larger

discrepancy was in the pre-yield stress paths of some undrained specimens, an aspect that is difficult to reproduce (see e.g. [6]) and that may be improved by a more complex elastic model (anisotropic).

Table 3 CASM full parameter set for Porto silty sand

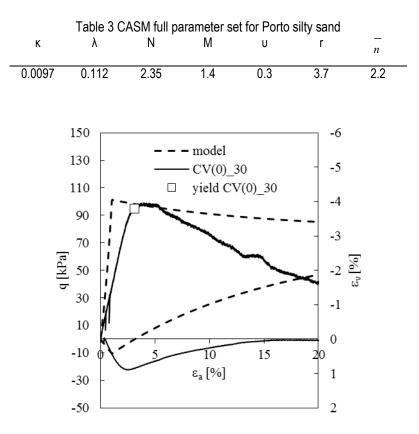| κ	λ	N	M	υ	r	$\bar{n}$
0.0097	0.112	2.35	1.4	0.3	3.7	2.2

Figure 4 Performance of the calibrated CASM model on drained triaxial tests on uncemented specimens. Circles indicate estimated yield point.
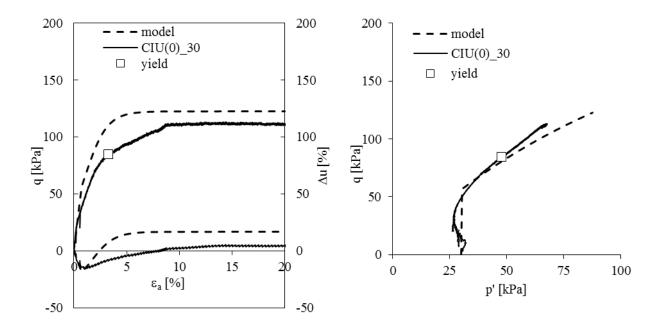

Figure 5 Performance of the calibrated CASM model on undrained triaxial tests on uncemented specimens. Squares indicate estimated yield point.

C-CASM: Initialization of b

The extension of CASM to cemented materials is based in the introduction of bonding (b) which is related to two different variables, p'_c and p'_t, controlling the isotropic compression yield and the tensile yield of the soil, respectively. This state variable should be related to a mixture ratio to ease initialization. This is done here using the results from isotropic compression paths. Experimental yielding points on isotropic compression tests provided p'_{c0}. Independently, the initial void ratio, e_0, provided a value of p'_{s0} using equation (9) as described previously. From these independent measurements, all the initial state values could be established as collected in Table 4.

Several relations between the initial state variables and different mixture ratios were explored. The best correlation (Figure 6) was obtained between $p_{s0}b_0$, the initial excess isotropic strength induced by cementation and the [21] mixture ratio ($n/C_{iv}^{0.21}$) in the form of a potential relation,

$$p_{s0}b_0 = c_1 \left(n/C_{iv}^{0.21} \right)^{c_2}$$

(10)

with c_1=9.95e9 kPa and c_2=-4.265. This correlation was used to identify the initial level of bonding for all the other numerical simulations in this work.
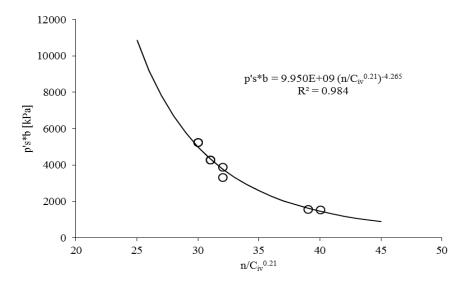

Figure 6 Relationship between the enlargement of the yield surface due to bonding and the mixing ratio

Table 4 Model state variables and initial values – Isotropic tests on cemented specimens

Test	e_0	%C	$n/C_{iv}^{0.21}$ [-]	p'_0 [kPa]	p'_{s0} [kPa]	p'_{c0} [kPa]	b_0 [-]	h_1 [-]
ISO(2)	0.71	2	40	1	517	2065	3.00	7
ISO(4)	0.78	4	39	1	274	1850	5.75	9
ISO(5)	0.64	5	32	1	1044	4383	3.20	3
ISO(7)	0.70	7	32	1	596	4500	6.55	7
CIU(5)_10000	0.60	5	31	1	1558	5842.5	2.75	1
CIU(5)_20000	0.60	5	31	1	1558	5842.5	2.75	1
CIU(7)_10000	0.65	7	30	1	955	5252.5	4.50	3
CIU(7)_20000	0.65	7	30	1	955	5252.5	4.50	3

Calibration of bonded-soil C-CASM parameters

The remaining task was to calibrate the model parameters specific to C-CASM: h_1, h_2 and α. As shown by eq. (8) h_1 controls the influence of volumetric plastic strain in bonding damage. The post peak response of the isotropic compression paths was used to calibrate this parameter for which a value $h_1 = 8$ was able to produce an adequate fit in most cases. In Figure 7 an example is provided.

It is also shown in Figure 7 how a better fit to the experimental curves could be obtained if the parameter h_1 is freely adjusted in each test. It was more surprising to find that this variation in the adjusted h_1 values was not random. Indeed, it was observed that the best fitting h_1 values were strongly correlated with the initial void ratio e_0 (Figure 8). For higher initial void ratios a higher h_1 is needed in order to better capture the post yielding behaviour. This linear relationship between the initial void ratio and h_1 was used in all the following numerical tests.
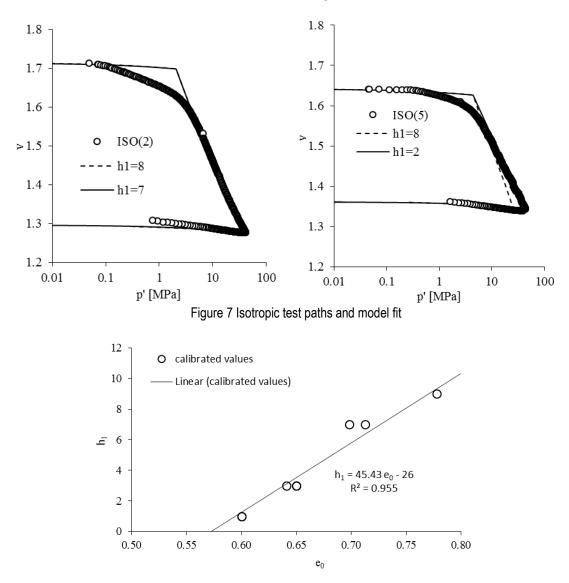

Figure 7 Isotropic test paths and model fit

Figure 8 Dependency of best-fit parameter h_1 on initial void ratio

Clearly, it would be preferable to have all model parameters independent of initial state. Therefore, the finding that h_1, the parameter controlling volumetric damage, increases with initial

void ratio, points to a shortcoming in the model formulation. It suggests that a more complex state equation than (7) above, perhaps including the other state variable, p_s should control bonding degradation. Micromechanical studies or multiscale modelling approaches such as those presented by [10] and [25] respectively, are likely to be useful in this respect.

Estimates of the parameter (α) controlling tensile strength can be easily obtained from a drained triaxial compression test. Peak strengths values are easily identified in this kind of test. Within the model that peak corresponds to the onset of yielding. Following the effective stress path of a drained triaxial test it is possible to write that:

$$p'_{peak} = p_{cell} + \frac{q_{peak}}{3} \tag{11}$$

And when yielding occurs f=0, hence:

$$f = 0 = \left[\frac{q_{peak}}{M\left(p_{cell} + \dfrac{q_{peak}}{3} + \alpha b_0 p_{s0} \right)} \right]^n + \frac{1}{\ln r} \ln \left[\frac{p_{cell} + \dfrac{q_{peak}}{3} + \alpha b_0 p_{s0}}{(1 + b_0 + \alpha b_0) p_{s0}} \right] \tag{12}$$

From this analytical expression, given the CASM parameter values (M, $\overline{n}$, r) and the initial state (p_{s0}, b_0) of the specimen a value of α can be obtained for each test. This procedure was applied to all the drained triaxial tests on the database–except those used below for validation purposes. The α values deduced showed some variability, but there was no correlation with void ratio or any other state variable. Discarding outliers (i.e. values exceeding by more than 2 standard deviations the initial mean value) a mean value of 0.27 was assigned to the tensile strength parameter (α).
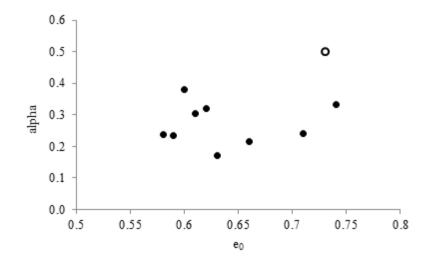

Figure 9 Initial void ratio vs estimated values of α parameter (empty symbol: outlier)

The final parameter to be calibrated was h_2, which controls the shear induced degradation of bonding. That was calibrated using the results of two undrained triaxial shear tests at large pressure. Several hypotheses were explored. [26] indicated that for structured clays $h_1 \approx 3\, h_2$;

a rule also applied by [18] using C-CASM. On the other hand, various researchers (e.g. [6]) assume that the contribution of shear and volumetric plastic strain to bond damage is equal. In this model that would mean $h_1 = h_2$. The simulations performed in this case (Figure 10) indicated that neither of these simplifying rules was of application here: $h_1 \approx 3\ h_2$ performed poorly on test CIU(5), whereas $h_1 = h_2$ was not adequate for test CIU (7). It was observed that the best join fit was obtained when h_2 was assumed as a constant equal to 1, independently of the void-ratio dependent value of h_1. In Table 5 the final set of adjusted parameters is reported.
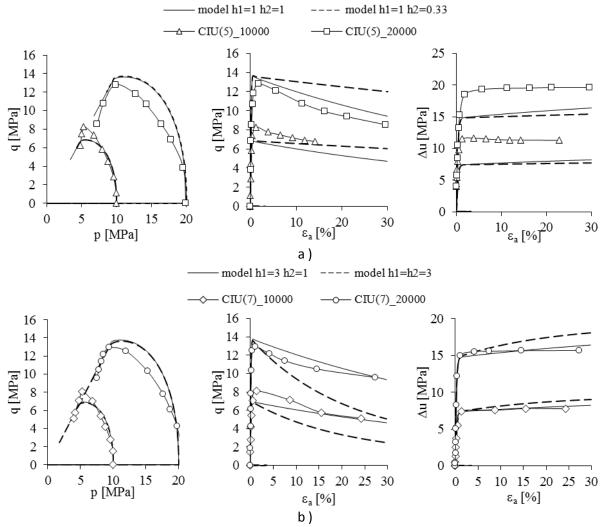

Figure 10 Calibration of parameter h_2 on high pressure undrained triaxial tests. Red-discontinuous line: discarded adjustment. Black-continuous line: final fit. (a) Specimens with cement content C = 5% and moulding void ratio $e_0 = 0.60$; b) specimens with cement content C = 7% and moulding void ratio $e_0 = 0.65$
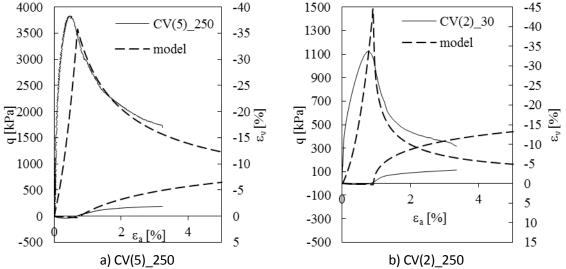
Table 5 C-CASM full parameter set for Porto silty sand

κ	λ	N	M	υ	r	$\bar{n}$	$α_t$	h_1	h_2
0.0097	0.112	2.35	1.4	0.3	3.7	2.2	0.27	$(45\ e_0 - 26)^*$	1

* from Figure 8

Validation of the calibrated C-CASM

The calibrated model is now validated by simulating several drained and undrained low confinement pressure triaxial compression tests (Figure 11). Parameters and initial conditions of these tests are reported in Table 6. The tests selected for validation, covering both the high and low mixture ratios, were different from those previously used for parameter adjustment. For the two drained simulations, the stress-strain response is presented, while for the two undrained simulations, the excess water pressure and the stress path in the triaxial plane are also shown. Discrepancies with the undrained response have several sources. As before, lack of elastic anisotropy in the model is important pre-yield. Post-yield, brittle localization of the experimental specimens was not simulated: this experimental response is quite sensitive to small sample imperfection and localized pore pressure response [21]. Despite these limitations the comparison indicates that C-CASM model correctly reproduces the treated soil behaviour. This is particularly so for the post-peak softening in drained response, a feature that is important in progressive failure of geotechnical structures beyond the capabilities of the frequently used Mohr-Coulomb model.

Table 6 Model state variables and initial values of the cemented specimens selected for calibration

Test	e_0	%c	$n/C_{iv}^{0.21}$ [-]	p'_0 [kPa]	$p_{s0}b_0$ [kPa]	p_{s0} [kPa]	b_0 [-]	$h_1(e_0)$ [-]
CV(2)_30	0.61	2	37	1	2039	1413	1.4	1.7
CV(5) - 250	0.58	5	30	1	4988	1894	2.6	0.3
CIU(2)-250	0.60	2	37	1	2039	1558	1.3	1.0
CIU(5)-250	0.58	5	30	1	4988	1894	2.6	0.6

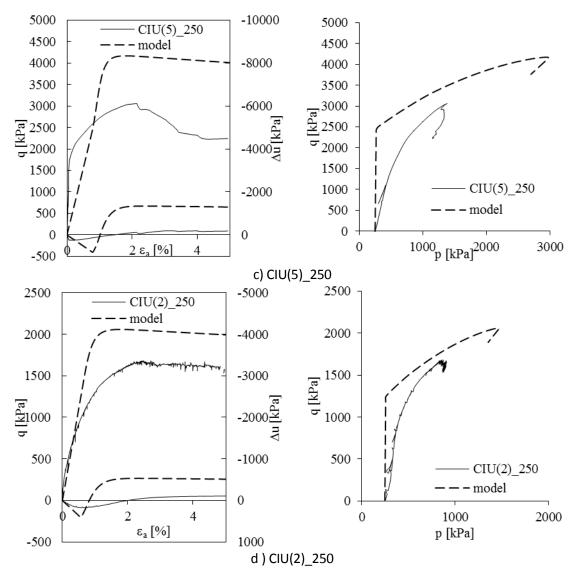a) CV(5)_250   b) CV(2)_250

Figure 11 Triaxial test results and model predictions for drained and undrained triaxial tests: a) Drained test on specimen with cement content C = 5% and moulding void ratio e_0 = 0.58; b) Drained test on specimen with cement content C = 2% and moulding void ratio e_0 = 0.61; c) Undrained test on specimen with cement content C = 5% and moulding void ratio e_0 = 0.58; d) Undrained test on specimens with cement content C = 2% and moulding void ratio e_0 = 0.60;

Discussion

Initialization of the bonding state, b is a key element for the application of this model. Here, a function linking initial bonding to the mixture ratio ($n/C_{iv}^{0.21}$) was obtained by inspection of yielding points on isotropic compression, some of them at relatively large stresses. Reproducing that procedure for other material would be costly and a simpler procedure is desirable.

[5], working with cemented Bangkok clay, obtained a similar relationship between extra initial isotropic strength ($p'_{so}b_0$) and the relevant mixture ratio for that material. The relation was there exponential instead of potential as it is here and the controlling mixture ratio was different (e_{0t}/A_w). Generalizing it can be said the kind of relation sought can be described by a generic function F of a mixture ratio, X,

$$p'_s b = F(X)$$ (13)

[5] went on to show that the function *F* that was obtained using isotropic yield, could be also deduced from much cheaper UCS results, with a relation, *A*, that was given by some model parameters and was only slightly dependent on *b*,

$$q_u = A F(X)$$ (14)

$$A = M \alpha_t \left(-\frac{1}{\ln r} \ln \frac{\alpha_t b}{1 + b + \alpha_t b} \right)^{1/\bar{n}}$$

Using the parameters M, $\bar{n}$, r and α_t reported in Table 5, A was re-evaluated for this work and its was concluded that for the relevant range of initial b values, A ≈ 0.42.

If F(X) in equation (15) is replaced by equation (10), this will imply that a good fit to the UCS data for this material should be obtained using,

$$q_u = A c_1 \left(\frac{n}{C_{iv}^{0.21}} \right)^{c_2} = 4.2 * 10^9 \left(\frac{n}{C_{iv}^{0.21}} \right)^{-4.265}$$ (15)

Indeed, this expression is very close to the optimal fit between UCS and the mixture ratio ($n/C_{iv}^{0.21}$) previously obtained from laboratory data [21]. This suggests that, at least for preliminary purposes, the relation necessary for bonding initialization can be advantageously deduced from a suite of UCS tests.

Some triaxial testing of the cemented soil would still be necessary to adjust the bonded soil parameters, h_1, h_2 and α. Ideally, this shall include one isotropic or oedometric test, plus one undrained and one drained triaxial test. This testing suite does not need to be replicated at different mixture ratios.

Conclusions

The main conclusions of the work presented are:

1. The C-CASM model did reproduce correctly the mechanical behaviour of compacted cemented Porto silty sand, thus showing that a model previously applied for cemented clays is also suitable for compacted sands.
2. The two state variables that, apart from effective stress, control material behaviour in C-CASM can be initialized knowing porosity and cement content. The relation between these physical measures and bonding, as represented in the model, can be deduced from a suite of UCS tests. Empirical examination of that kind of tests should be also enough to identify the controlling mixture ratio for the material.
3. 7 out of 10 parameters in C-CASM should be determined on the target untreated soil. They do not need high quality samples, because reference behaviour is unstructured. The remaining three parameters would require a moderate amount of triaxial testing on a single mixture.

It is hoped that the work exemplified here will encourage a more widespread application of advanced soil models in numerical assessment of cemented-soil structures.

Acknowledgments

References

[1]   Croce P, Flora A, Modoni G. Jet Grouting: Technology, Design and Control. CRC Press; 2014.

[2]   Hajiabdolmajid V, Kaiser PK, Martin CD. Modelling brittle failure of rock. International Journal of Rock Mechanics and Mining Sciences 2002; 39(6):731-741.

[3]   Yapage NNS, Liyanapathirana DS, Kelly RB, Poulos H G, Leo CJ. Numerical Modelling of an Embankment over Soft Ground Improved with Deep Cement Mixed Columns: Case History. Journal of Geotechnical and Geoenvironmental Engineering 2014; 140(11), 04014062

[4]   Namikawa T, Mihira S. Elasto-plastic model for cement-treated sand. International journal for numerical and analytical methods in geomechanics 2007; 31(1):71-107.

[5]   Arroyo M, Ciantia M, Castellanza R, Gens A, Nova R. Simulation of cement-improved clay structures with a bonded elasto-plastic model: A practical approach. Computers and Geotechnics 2012; 45:140-150.

[6]   Chen Q, Indraratna B, Carter J, Rujikiatkamjorn C. A theoretical and experimental study on the behaviour of lignosulfonate-treated sandy silt. Computers and Geotechnics 2014; 61:316-327.

[7]   Lagioia R, Nova R. An experimental and theoretical study of the behaviour of a calcarenite in triaxial compression. Géotechnique 1995, 45(4):633-648.

[8]   Rouainia M, Muir Wood D. A kinematic hardening constitutive model for natural clays with loss of structure. Géotechnique 2000, 50(2):153–64.

[9]   Gonzalez NA, Rouainia M, Arroyo M, Gens A. Analysis of tunnel excavation in London Clay incorporating soil structure. Géotechnique 2012; 62(12):1095-1109.

[10]   Ciantia M O, di Prisco C. Extension of plasticity theory to debonding, grain dissolution and chemical damage of Calcarenites. International Journal of Numerical and analytical methods in Geomechanics 2015. (accepted)

[11]   Han J, Oztoprak S, Parsons RL, Huang J. Numerical analysis of foundation columns to support widening of embankments. Comput. Geotech 2007; 34 (6):435–448.

[12]   Ignat R, Baker S, Larsson S, Liedberg S. Two-and three-dimensional analyses of excavation support with rows of dry deep mixing columns. Computers and Geotechnics 2015, 66:16-30.

[13]   Yu HS. CASM: A Unified state parameter model for clay and sand. International Journal for Numerical and Analytical Methods in Geomechanics 1998, 22:621-653.

[14]   González N, Arroyo M, Gens A. The effect of structure in pressuremeter tests in clay. Nu[5]merical Models in Geomechanics, NUMOG X, Pande & Pietrusckzak (eds) 2007; 721-732.

[15]   Yu HS, Tan SM, Schnaid F. A critical state framework for modelling bonded geomaterials. Geomechanics and Geoengineering 2007; 2(1):61-74.

[16]   González NA. Development of a family of constitutive models for geotechnical applications. Ph. D. Thesis. Barcelona, Spain: Technical University of Catalonia, UPC 2011

[17]   Arroyo M, González N, Butlanska J, Gens A, Dalton C. SBPM testing in Bothkennar clay: structure effects. Geotechnical and geophysical site characterization 2008, Taylor & Francis Group, London, 456-462.

[18]   González NA, Arroyo M, Gens A. Identification of bonded clay parameters in SBPM tests: a numerical study. Soils and Foundations 2009, 49(3):329-340

[19]   Gens A, Nova R. Conceptual bases for a constitutive model for bonded soils and weak rocks. Geotechnical Engineering of Hard soils - Soft Rocks, Anagnostopoulos et al. (eds) 1993. Balkema, Roterdam

[20]   Viana da Fonseca A, Carvalho J, Ferreira C, Santos J A, Almeida F, Pereira E, Feliciano J, Grade J, Oliveira A. Characterization of a profile of residual soil from granite combining geological, geophysical, and mechanical testing techniques. Geotechnical and Geological Engineering 2006, Springer, Netherlands, 14(5):1307-1348

[21]   Rios S, Viana da Fonseca A, Baudet BA. The effect of the porosity/cement ratio on the compression of cemented soil. Journal of Geotechnical and Geoenvironmental Engineering 2012, 138(11):1422–1426.

[22]   Rios S, Viana da Fonseca A, Baudet BA. On the shearing behaviour of an artificially cemented soil. Acta Geotechnica 2014, 9(2):215-226.

[23]   Amaral MF. Modeling and characterization of the dynamic and cyclic behavior of soil-cement admixtures to apply in transport infrastructures. Ph.D. Thesis, University of Porto 2012.

[24]   Amaral MF, Da Fonseca AV, Arroyo M, Cascante G, Carvalho J. Compression and shear wave propagation in cemented-sand specimens. Géotechnique Letters 2011, 1 (July-September), 79-84.

[25]   Jiang M, Zhang F, Sun, Y. An evaluation on the degradation evolutions in three constitutive models for bonded geomaterials by DEM analyses. Computers and Geotechnics 2014, 57:1-16.

[26]   Callisto L, Rampello S. An interpretation of structural degradation for three natural clays. Canadian Geotechnical Journal 2004, 41(3):392-407.